JOURNAL OF MATERIALS SCIENCE 31 (1996) 5961–5973

Titanium diboride particle-reinforced aluminium with high wear resistance

A. V. SMITH, D. D. L. CHUNG
Composite Materials Research Laboratory, State University of New York at Buffalo, Buffalo, NY 14260-4400, USA

A TiB_2 particle (61 vol %, 4 μm mean size) reinforced aluminium fabricated by liquid-aluminium infiltration was subjected to unlubricated rolling wear and was found from the weight loss to be 1.5 times more wear resistant than 17-4 ph stainless steel, twice as wear resistant as 1020 steel, 7.5 times more wear resistant than 2024 aluminium, and 12.8 times more wear resistant than the aluminium matrix. This wear resistance is attributed to the lack of particle pull-out and the ability of the TiB_2 particles to protect the softer underlying matrix from abrasion. This composite was approximately three times more wear resistant than AlN particle (50 vol %)-reinforced aluminium. The greater wear resistance of Al/TiB_2 compared to Al/AlN is due to the slow wear of the TiB_2 particles and the AlN particle pull-out. A slight decline in tensile strength and no effect on the modulus was observed in Al/TiB_2 after heating at 300 or 600 °C for 240 h. This high-temperature stability is attributed to the lack of reactivity between TiB_2 and the aluminium matrix.

1. Introduction

Wear resistance is becoming more critical as the need for lightweight, long-lasting components is increasing. A large part of the driving force for this phenomenon is the need to lower the impact of combustion processes, such as automotive [1] and jet aircraft engines, on the environment. Although much emphasis has been placed on these transportation-oriented applications, aluminium-matrix composites are slowly infiltrating other applications. Examples of these other applications are air-conditioning vanes [2], bearings, and automotive brake components [3]. Aluminium-matrix composites are very attractive for these applications. By being lower in weight than the steel parts that are traditionally used in these applications, aluminium-matrix composites hold the promise of raising fuel economy and thus reducing pollution from the resultant fuel savings. By judiciously selecting the reinforcements used in the aluminium matrix, the wear performance of composite parts can approach or exceed that of steel parts. This increased wear resistance of the aluminium-matrix composites alleviates the problems encountered when trying to substitute aluminium alloys for steel in moving-part applications [1].

An objective of this study was to develop an aluminium-matrix composite with wear resistance superior to plain low-carbon steel and stainless steel. Materials that exhibit high wear resistance, together with high-temperature resistance, can increase machinery efficiency by maintaining design tolerances longer than unreinforced materials. Ceramic-reinforced aluminium composites offer increased wear resistance, especially over unreinforced aluminium alloys [1, 2, 4]. For example, alumina-reinforced aluminium used as automotive engine pistons results in increased power output along with a longer component life [5].

Although wear resistance is important for increasing the efficiency of automotive and aerospace engines, relatively little information is available on the wear properties of aluminium-matrix composites [1]. Previous study [6] of the wear of Al/TiB_2 particle composites pertains to composites with $\leqslant 10$ vol % TiB_2 particles. This study attempts to increase the available rolling wear information on aluminium-matrix composites; specifically, wear results for a composite with a TiB_2 particle loading of approximately 61 vol % are presented.

The improved wear resistance of the particle-reinforced aluminium alloys aids more than just the moving parts of combustion engines. By providing a light weight alternative to cast iron in automotive brake rotors, the weight of automobiles can be reduced further [3]. An additional benefit to the replacement of cast iron in brake rotors with an aluminium-based composite is an increase in heat dissipation and thus an improvement in braking performance. Another reason for studying ceramic-reinforced aluminium-matrix composite wear, especially abrasive wear, is that a better understanding of composite machining can be gained [4].

Studies indicate that particles of both hardness extremes improve the wear resistance of aluminium alloys [1, 7]. Hard ceramic particles (e.g. SiC, Al_2O_3, silica, B_4C and TiB_2) [7] and soft solid lubricants (e.g. graphite and MoS_2) [7] have been used to increase the wear resistance of the aluminium matrix. Hard and soft particles involve different mechanisms for increasing the wear resistance of a composite. Hard particles increase wear resistance by wearing at a much lower

0022–2461

rate than the matrix. The protruding hard particles support the counter surface away from the softer matrix and thus reduce the rate at which the matrix is worn. Soft particles tend to smear over the aluminium matrix surface, acting as a solid lubricant. A disadvantage of soft particles is the loss of mechanical strength that the matrix experiences when the lubricating particles are introduced [7, 8]. Combined use of both hard and soft particles in the same aluminium-matrix composite has also been reported [8, 9].

Most previous studies of composite wear concentrated on composites with low volume fractions ($< 20\%$) of particles [1, 7]. Lee *et al.* [1] mention hard-particle composites with volume fractions up to 40% and soft-particle composites, fabricated by powder metallurgy, up to 80%. Although wear testing of hard-particle composites at 20 vol % or less has been previously reported, that of composites at > 20 vol % has not. Moreover, wear testing has not been reported on AlN particle-reinforced aluminium at any volume fraction. As previously discussed, wear data for $\leqslant 10$ vol % TiB_2 particle-reinforced aluminium composites have been reported [6]. This work reports on the wear resistance of TiB_2 particle-reinforced aluminium with 61 vol % TiB_2 and AlN particle-reinforced aluminium with 50 vol % AlN. In contrast to SiC, both TiB_2 and AlN do not react with aluminium, so brittle reaction products at the reinforcement–matrix interface which harm the bonding are avoided. Al_2O_3 also does not react with aluminium, but it has been shown to be mechanically inferior to SiC or AlN as a reinforcement in aluminium [10].

There are many ways that wear can occur in a part. Therefore, many different types of wear tests have been developed to simulate different types of wear [4]. Some of the most important wear tests involve sliding, rolling, abrasion and scuffing. A sliding test involves a stationary surface, usually the material to be tested, and a second body in contact and moving relative to the first body (stationary surface). Wear on the first or second body can create a third body, i.e. loose wear debris that can interact with the first and second bodies if it is not removed. The stresses involved in the sliding wear tests are primarily static frictional stresses. These static stresses result from adhesion, abrasion, asperity interlocking or third-body forces [6]. There is a minor dynamic component to the sliding wear test due to dynamic interactions between the asperities [6]. Although little research has been done on metal-matrix composite sliding wear mechanisms, evidence to date suggests that composite wear mechanisms are similar to those for unreinforced metals [4]. Typical sliding tests are the pin-on-disc test [2] and the block-on-ring test [9].

In a rolling test, one or both surfaces are moving relative to the other. Relatively little, if any, sliding occurs. Again, third-body wear can occur. Rolling wear differs from sliding wear in that the frictional forces are much lower and cyclic loading is an important factor [6]. This type of loading is often seen in ball or roller bearings [4]. In the leading edge of the wheel or cylinder in contact with the first body, compressive forces occur, whereas the trailing edges are affected by tensile forces [6]. This appears to induce fatigue in the sample surface [6]. It has been suggested that aluminium alloy metal-matrix composites are poor candidates for rolling wear applications [4]. This is due to failure at the ceramic/matrix interface when exposed to rolling cyclic contact, akin to the failure in tensile fatigue [4]. Because TiB_2 does not form brittle interfacial compounds with molten aluminium, this reinforcement is a good candidate for avoiding such failure when subjected to rolling wear. A wide variety of materials, ranging from hardened steels to bonded carbides, can be used for the rotating wheels. Typical rolling tests involve a rotating wheel on a rotating platform or a roller on a cylinder [9].

Abrasive wear involves the introduction of abrasive particles between the first and second body. Often the second body is made of a compliant material, such as rubber, so that the second body only supplies normal forces to the wear process. This is to allow evaluation of the effect of the abrasive particles independent of any second-body effects. Typical abrasive wear tests is the rubber wheel abrasion test [11] and the spindle wear test [1].

Scuffing wear primarily occurs between parts such as pistons and cylinders or pistons and piston rings of an internal combustion engine. Scuffing involves the transfer of mass from the surface of one body on to the surface of another [12]. This produces scratches and localized welding of the transferred material [12]. Third-body wear is not usually involved.

In addition to the types of wear discussed above, other variables can affect the amount of wear. One variable in studying wear is the type and amount of lubrication (or lack of lubrication) used between the bodies involved. Another variable is the load that the bodies experience at the point of wear. With all these variables affecting both real wear applications and wear tests, it is difficult to compare the results of different wear test studies. This study concentrates on unlubricated rolling wear subjected to a 9.8 N force, similarly performed on Al/TiB_2 and Al/AlN composites.

The retention of mechanical properties at elevated temperatures is an important goal for present-day materials research. Maintaining a high percentage of the room-temperature properties of materials at elevated temperatures is important in the areas of jet aircraft engine design, internal combustion engines, aerospace structures, and military applications. In many of these fields, the inability to achieve higher efficiency machines is not hampered by the existing underlying technologies, but instead by the lack of lightweight, strong materials, the properties of which do not degrade with increasing temperature.

Ceramic particle-reinforced aluminium offers the promise of greatly increasing the strength of the matrix and, with proper selection of the reinforcement, can offer resistance to degradation of the mechanical properties at high temperatures. With the above discussion in mind, another objective of this study was to develop an aluminium-matrix composite that can withstand exposure to high temperatures.

Composites that show resistance to property degradation at high temperatures are often credited with having little or no chemical reactions between the matrix and the reinforcement [13, 14]. The most common ceramic reinforcement used in metal-matrix composites is SiC, which reacts with aluminium to form multiphase interfaces [15]. These interfacial compounds are often brittle and high in interfacial energy, so they degrade the mechanical properties of the composite [15]. There is also potential for growth of the interfacial phase with long-term high-temperature exposure of the composite. This growth can lead to degradation of the mechanical properties after long-term exposure to high temperatures. Examples of reinforcements that do not react with aluminium are AlN, Al_2O_3 [14] and TiB_2 [15].

TiB_2 was selected for this study owing to its reported resistance to chemical reaction with aluminium [15] and its ability to greatly enhance the wear resistance of the aluminium matrix [15]. TiB_2 was also selected as the reinforcement for aluminium because relatively little literature is available on the subject. Data on TiB_2 particle-reinforced aluminium have been reported for rolling wear [6], sliding wear [16] and mechanical properties [17]. In addition, the Al/TiB_2 interface was also studied [15].

The selection of the matrix was based on density, melting point, ease of fabrication, and commercial availability. Aluminium is a common lightweight metal. Improvements in room-temperature and elevated temperature mechanical properties and wear resistance may allow aluminium alloys to replace heavier materials in many weight-sensitive applications.

Pure aluminium matrix was chosen mainly because of its high ductility. A low-ductility matrix leads to low strength and low ductility in the composite [14]. It was also advantageous to select an aluminium alloy that was known not to react with TiB_2. Because the lack of interfacial reactions between reinforcement and matrix has been reported to enhance the mechanical properties of composites after long-term exposure to high temperatures, the aluminium alloy selected for consideration should be as close to pure aluminium as possible. This was to avoid potential side reactions from alloying elements. Aluminium alloy 170.1 was selected; it is commercially pure (99.70 wt % Al).

A third goal of this study was to compare the mechanical properties and wear test results of TiB_2 reinforced aluminium to other composites and engineering materials. Emphasis was placed on comparing the ultimate tensile strength and modulus of elasticity of TiB_2-reinforced aluminium to SiC-reinforced and AlN-reinforced aluminium. Comparing the mechanical properties at elevated temperatures between TiB_2- and SiC-reinforced aluminium was used to show the increase in high-temperature properties inherent in using non-reactive reinforcements, such as TiB_2, versus reactive reinforcements, such as SiC. Comparison with AlN (also non-reactive with aluminium)-reinforced aluminium was made in terms of wear-test properties and elevated-temperature resistance.

2. Experimental procedure

2.1. Materials

The alloy used in this study is an Alcoa foundry ingot alloy. It is referred to as aluminium rotor alloy 170.1. It contains 99.70 wt % Al. The melting point is 660 $\pm$1 °C. The tensile strength, modulus and ductility are 69 (5) MPa, 80 (9) GPa and 52% ($\pm$ 9%) (standard deviations in parentheses), as obtained by tensile testing four tensile bars made from the same ingot (as-cast condition) used to prepare the composite samples. The dimensions of the tensile test bars are the same for ingot and composites, and are shown in Fig. 1.

The reinforcement used in this study was a particulate ceramic, namely TiB_2. It was supplied by Advanced Ceramics Corporation, formerly Union Carbide/Praxair Advanced Ceramics, Cleveland, OH. The grade supplied by Advanced Ceramics Corporation for this study is referred to as HCT-F. It is a high-purity extremely fine ceramic particle. Previous studies of low-concentration TiB_2-reinforced commercial aluminium alloys have shown that the TiB_2 particles have no observable propensity to form interfacial products with the aluminium matrix [6, 15, 18]. One of these studies [18] contains photomicrographs of low-concentration TiB_2-reinforced aluminium where no discernible reaction products can be seen. The crystalline structure of TiB_2 is hexagonal.

The TiB_2 particles are produced by direct and continuous synthesis, in which carbothermal high-temperature reduction occurs. The resulting TiB_2 particle agglomerates are then milled to separate the individual particles [19]. The resulting particles are polycrystalline in nature. The mean particle size is 3–5 μm, as determined by the Microtrac Method [20]. The particles ranged in size from 0.5 to about 7.5 μm, with no particles over 10 μm in size [20]. The particles appeared to be platelets. The particle surface area was 1.0 $m^2 g^{-1}$ [20]. The result of chemical analysis is shown in Table I. The ultimate tensile strength of a polycrystalline platelet form of TiB_2 is 1177 MPa [17]. The modulus of elasticity of TiB_2 is 570 GPa [21]. Other literature sources list the modulus of elasticity as 530 GPa [16] and 531 GPa [17]. The manufacturer did not supply any mechanical property data. Although the fracture strain of polycrystalline TiB_2 platelets has not been reported, the fracture strain of a bulk TiB_2 crystal is 0.25% [17]. The Poisson's ratio of what is assumed to be a sintered TiB_2 of maximum theoretical density and 6.0 μm grain size is 0.10 [16]. The density of TiB_2 is 4.51 $g cm^{-3}$ [18].

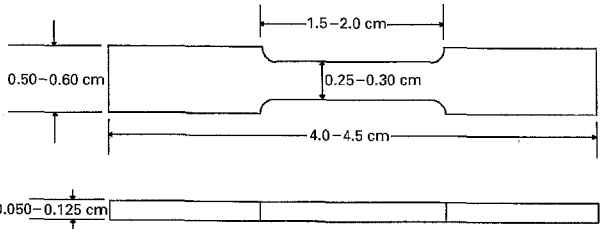

Figure 1 The tensile test bar.

TABLE I Typical chemical analysis (wt%) of the titanium diboride reinforcement, from [20]

Ti	B	Fe	Ni	Zn	Cu	Mg	Mn	Cr	Ca	V	Co	C	O	N	Mo	Zr	Na	Ni	W
67–69	29–32	0.03	[a]	[a]	0.50	[a]	[a]	[a]	[a]	[a]	[a]	0.50	1.0	0.20	[a]	0.015	[a]	[a]	[a]

[a] Not able to be detected at or below 30 p.p.m, as determined by ICP emission spectroscopy.

2.2. Composite fabrication

A steel mould was preheated to drive off any moisture that might have accumulated. Then the reinforcement was loaded into the mould. The reinforcement particles were lightly tapped down with a spatula and the mould was lightly pounded on a table to increase compaction. This was done to produce an interlocking free-standing and binder-free preform in the mould. A round piece of ceramic cloth was placed on top of the reinforcement preform. A solid bar of the matrix alloy was then placed on the cloth. The mould was then dried at 200–300 °C to drive off any moisture in the particular reinforcement. The mould, while still hot, was placed within the heating chamber for liquid-aluminium infiltration.

Before the mould that had been loaded into the heating chamber was heated to the melting point of the matrix, the space between the particles was evacuated in order to aid subsequent infiltration of the molten matrix. The chamber and mould were then subjected to multiple vacuum and inert-gas purge cycles until a satisfactory vacuum was achieved. The following purge cycle was typical and was repeated three times before beginning the heating cycle. The heating chamber was evacuated to a pressure of 500 mtorr (66.7 Pa). The chamber was then backfilled with argon to a pressure of 1.7 MPa. After the last argon purge, the lowest possible pressure (as low as 45 mtorr or 6 Pa) was re-established before starting the heating cycle.

The apparatus used for this study had a programmable heating and cooling cycle controller. The heating and cooling cycle used to produce the composite samples is graphically shown in Fig. 2, where the solid line represents the supply of thermostatically controlled power to the heating elements and the dashed line represents the pressure. The mould in the chamber was heated by an electrical resistance heating element while vacuum was maintained. Sufficient cooling was applied using a water jacket surrounding the heating chamber.

The first step in the heating cycle was to heat the mould to a temperature below the melting point of the matrix, and to dwell at this temperature. As can be seen in Fig. 2, in the first half hour the temperature in the heating chamber was raised to the first step temperature of 350 °C, which was maintained for half an hour. This segment of the heating and cooling cycle was used to allow any residual moisture to outgas before reaching the melting point of the matrix. The temperature was then rapidly raised above the melting point of the matrix in order to melt the matrix material and to supply superheat (and hence fluidity) to the molten matrix. The ultimate temperature achieved was 780 °C.

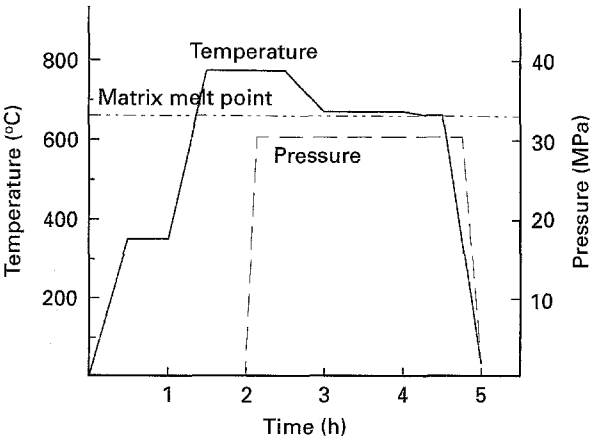

Figure 2 Graphical representation of the heating and pressure cycles in composite fabrication.

As the temperature exceeded the melting point of the matrix, the ingot of matrix above the reinforcement began to melt. When melting was complete, the matrix formed a molten pool above the reinforcement. This molten pool sealed off the vacuum in the space between the particles of reinforcement. After the molten matrix had attained a sufficient amount of superheat, a pressure great enough to overcome the forces opposing the infiltration of the matrix into the reinforcement was applied isostatically within the heating chamber. High-pressure argon gas flow was introduced after half an hour at the ultimate temperature. The maximum pressure this gas reached was 30.6 MPa. One of the reasons that a high infiltration pressure of 30.6 MPa was selected to produce the TiB_2-reinforced aluminium was to achieve a highly (essentially 100%) infiltrated composite. This high infiltration pressure was necessary owing to the small diameter of the infiltration paths resulting from the small particles used in this study.

It is interesting to note that the AlN particles of a previous study [14] are of a similar particle size as the TiB_2 used in this study, yet they required higher infiltration pressures (in excess of 41 MPa) to approach complete infiltration. This appears to be due to the greater wettability of TiB_2, as compared to AlN, by molten aluminium [15].

After a sufficiently long infiltration time, the heating chamber was cooled until the composite and mould were sufficiently cooled for removal. This was accomplished by discontinuing heating of the chamber and mould, while continuing use of the water jacket.

2.3. Mechanical testing

Tensile test samples were produced from composites manufactured for this study. These samples were

TABLE II Tensile test results for TiB_2 (61 vol %) aluminium-matrix composite

	As-fabricated	300 °C[a]	600 °C[a]
Strength (MPa)	414 (24.9)	351 (91.5)	374 (63.7)
Modulus (GPa)	160 (14.2)	171 (56.4)	222 (40.0)
Elongation (%)	0.17 (0.06)	0.16 (0.03)	0.13 (0.01)

[a] Tested at room temperature after heating.
Note: Standard deviation shown in parentheses. Each data point is the average of the data of three test samples.

diamond saw sectioned and abrasively ground to the dimensions shown in Fig. 1. The samples were then tested using a Sintech 2/D 9000 N capacity mechanical testing machine. The strain was measured with strain gauges (type EA-13-120LZ-120) supplied by Measurements Group, Inc.

A qualitative observation was made during diamond saw sectioning. Sectioning of similarly sized Al/SiC and Al/AlN composites produced on the same equipment by other researchers [10, 13, 14] required approximately 1–2 h per complete sectioning cut. The same length cut for the Al/TiB_2 composite of this work required approximately 4–8 h. This difficulty encountered in machining is consistent with the high wear resistance that the Al/TiB_2 composite exhibited.

The per cent elongation (Table II) was estimated from the strain at the break point. Because the software recorded the extension of the sample, by measuring the separation of the sample grips with time, the per cent elongation was obtained by dividing the sample extension by the sample length. The sample length exposed to elongation was measured in the reduced width part, ignoring the insignificant or negligible extension occurring in the wider ends confined by the test grips.

2.4. Wear testing

The rolling wear test was performed on a Teledyne Taber Model 503 abrasive tester. Fig. 3 is a drawing of the samples tested. A platform, shown in Fig. 4, was machined to hold the wear test samples. The platform rotated at 72 r.p.m., and the test was run for 240 h (10 days) for each sample. Two parallel abrasive wheels (6.5 cm from centreline to centreline) rode on the rotating platform and came into contact with the wear test samples. No lubrication was introduced. The resulting third-body particles, worn free from a sample or separated from the bonded silicon carbide wheels, remained in the wear track and interacted with the test sample and the bonded silicon carbide wheels. The wheels (1.3 cm wide) used to abrade the samples were made from bonded silicon carbide. These wheels and thus the samples were exposed to a 9.8 N force. The diameter of the sample that was inserted into the wear test fixture was 3.5 cm.

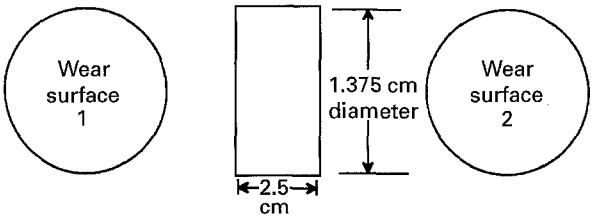

Figure 3 Wear-test sample geometry. This sketch is used to show which surfaces are wear tested for the two heat-treatment states of the Al/TiB_2 (61 vol %) composite. Face 1 was wear tested in the as-fabricated state. After heat treating at 600 °C for 240 h, face 2 was wear tested.

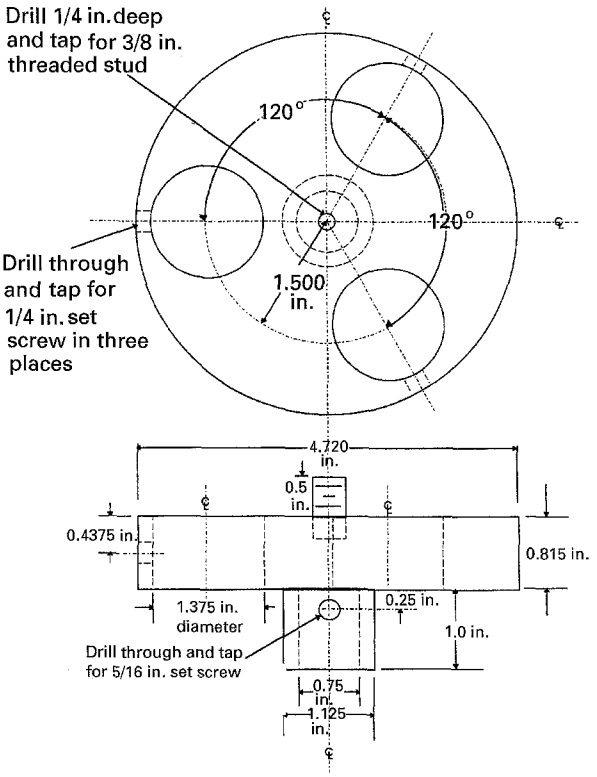

Figure 4 Wear-test fixture. 1 in ≃ 2.54 cm.

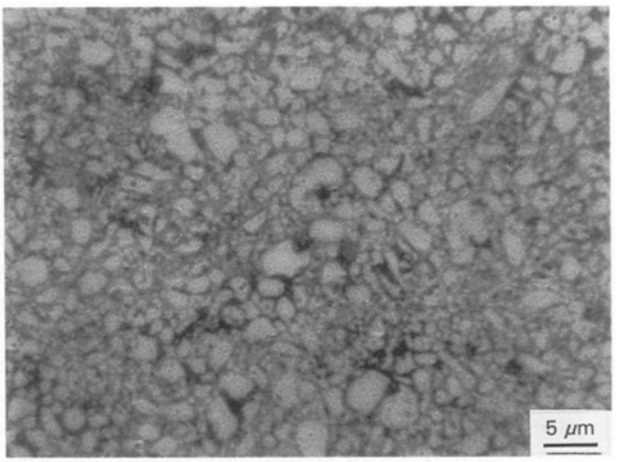

Figure 5 Scanning electron micrograph of as-fabricated Al/TiB_2 with 61 vol % TiB_2.

3. Results and discussion

3.1. Microstructure

The microstructure of Al/TiB_2 (after mechanical polishing) was studied to determine TiB_2 particle density and distribution. Fig. 5 shows a scanning electron micrograph of the as-fabricated Al/TiB_2 composite. The volume fraction of the particles in the composite was 0.61 for all sample conditions (as-received, after

TABLE III Comparison of ultimate tensile strength results for typical engineering materials and for TiB_2 (61 vol %) aluminium-matrix composite

	UTS (MPa)				
	As-fabricated[a]	300 °C[a,b]	600 °C[a,b]	O	T6
61 vol % TiB_2-reinforced Al	414	351	374	–	–
170.1 aluminium (as-fabricated)	69	–	–	–	–
2024 aluminium	–	–	–	179.3 [22]	475.7 [22]
1020 steel cold-rolled	413.7 [21]	–	–	–	–
17-4 ph stainless steel	–	–	–	–	655 [21]
W1 tool steel[c]	–	–	–	–	–

[a] Tested at room temperature after heating.
[b] Each data point is the average of the data of three test samples.
[c] Tool steels are not used for structural applications. Ultimate tensile strength is not a property listed for tool steels. Typical properties for tool steels are hardness with various heat treatments, and toughness values.

heating to 300 or 600 °C in air for 240 h), as determined by quantitative metallography.

3.2. Tensile properties

Table II shows the tensile test results of the Al/TiB_2 composite. Each value shown is the average of the test of three tensile bars. Included with the data are the standard deviations. There was about a 10–15% drop in ultimate tensile strength after the samples had been exposed to 300 or 600 °C for 240 h. This decrease did not become more severe with increase in temperature from 300 °C to 600 °C, indicating stability of properties with temperature increases up to 600 °C. One possible source of this decrease in strength after high-temperature exposure of the Al/TiB_2 composite could be the formation of brittle Al_2O_3. Aluminium oxide could form due to oxidation of the sample surface and may even be able to penetrate past the surface through cracks and pores, thus reducing the tensile strength.

The strength of Al/TiB_2 after exposure to temperatures approaching the melting point of pure aluminium was much higher than those of pure aluminium or traditional aluminium alloys after an identical heat treatment. Under the same heating conditions, the unreinforced aluminium matrix and aluminium alloys would experience significant grain growth, which results in a catastrophic loss of strength and an increase in brittleness. This ability to retain successfully a good portion of the composite's original strength after heat treatment may also indicate that Al/TiB_2 may have greater high-temperature strength than traditional aluminium alloys.

Table III compares the ultimate tensile strength of Al/TiB_2 and those of typical engineering materials. The Al/TiB_2 composite, even after exposure to high temperatures for long times, were equivalent in ultimate tensile strength to low carbon steel, which was slightly weaker than fully hardened 2024-T6 aluminium. Only 17-4 precipitation hardening (ph) stainless steel, in its fully hardened state, was significantly stronger than the Al/TiB_2 composite.

TABLE IV Comparison of metal-matrix composite ultimate tensile strength values[a]

	UTS (MPa)		
	As-fabricated	300 °C[b]	600 °C[b]
Al/TiB_2 61 vol %	414 (24.9)	351 (91.5)	374 (63.7)
Al/SiC 55 vol % [10]	313.0 (37.5)	–	257.2 (12.4)
Al/AlN 58.6 vol % [10]	300.9 (25.2)	–	–
Al/AlN 62 vol % [10]	430.3 (14.1)	422.9[c] (9.9)	400.9 (24.1)
Al/AlN 63.3 vol % [10]	406.3 (33.9)	–	–
Al/Al_2O_3 61.4 vol% [10]	275.8 (14.6)	–	198.6 (3.2)
Al/Al_2O_3 70.2 vol %[10]	237.8 (8.4)	–	–

[a] Standard deviations are shown in parentheses. For the TiB_2 samples, three tensile bars were tested.
[b] Tested at room temperature after heating.
[c] Exposed to 300 °C for 210 h, rather than 240 h for all other heated samples.

The original matrix material and the fully annealed 2024 aluminium alloy (heat-treatment condition O) both had lower ultimate tensile strength than the Al/TiB_2 composite. The fully precipitation hardened alloys were stronger or slightly stronger than the Al/TiB_2 composite. At least for the 2024 aluminium alloy, when subjected to annealing, the strength dropped below that of the Al/TiB_2 composite, though this is not shown in Table III.

Table IV compares the ultimate tensile strength of typical aluminium–matrix composites with the Al/TiB_2 (61 vol % TiB_2) composite. Note that the composites compared in this table all used the same matrix as Al/TiB_2. The AlN and TiB_2 composites of greater than 60 vol % reinforcement were approximately equivalent in ultimate tensile strength, even after heating at elevated temperatures. The 61 vol % TiB_2 composite was stronger than the approximately 55–59 vol % SiC or AlN composites. The 61 vol % TiB_2 composite was significantly stronger than the approximately 61–70 vol % Al_2O_3 composites. Also evident was a small decline in the ultimate tensile strength of both Al/TiB_2 and Al/AlN after exposure to high temperatures for long periods of time.

Table II shows the modulus of elasticity results for the tensile test samples. There was no trend towards

a change in the modulus of elasticity due to heat treatment at 300 or 600 °C for 240 h. This indicates a stability of the modulus of elasticity with exposure to relatively high temperatures for long periods of time.

Table V compares the modulus of elasticity of the Al/TiB_2 composite and those of typical engineering materials. The Al/TiB_2 composite was much stiffer than aluminium and aluminium alloys, and similar in stiffness to steel and stainless steel. This indicates that the reinforcement particles greatly increased the modulus of elasticity of the composite when compared to the aluminium matrix. As can be seen from Table V, there was no observable effect of long-term heat exposure on the modulus of elasticity.

Table VI compares the modulus of elasticity of various aluminium-matrix composites. The modulus of the elasticity of the composites was similar for TiB_2 and AlN reinforcements at similar volume fractions. Al/SiC with a lower (5 vol % lower) reinforcement volume fraction than Al/TiB_2 showed a modulus of elasticity that was greater than that of Al/TiB_2.

The per cent elongation (Table II) was low, whether with or without heating.

TABLE V Comparison of modulus of elasticity results for typical engineering materials and for TiB_2 (61 vol %) aluminium-matrix composite

	Modulus of elasticity		
	As-fabricated (MPa)	300 °C[a] (GPa)	600 °C[a] (GPa)
61 vol % TiB_2 composite	160	171	222
170.1 aluminium (as-fabricated) [23]	71	–	–
2024 aluminium [22]	73.1[b]	–	–
1020 steel cold-rolled [21]	208.6	–	–
17-4 ph stainless steel [21]	195.6	–	–
W1 tool steel[c]	–	–	–

[a] Tested at room temperature after heating.
[b] This value does not depend on heat treatment.
[c] Tool steels are not used for structural applications. The modulus of elasticity is not a property listed for tool steels. Typical properties for tool steels are hardness with various heat treatments, and toughness values.

3.3. Wear behaviour

Table VII shows unlubricated rolling wear test results for Al/TiB_2. For comparison, 1020 carbon steel, W1 tool steel, 17-4 ph stainless steel, 170.1 aluminium, 2024 aluminium and Al/AlN were also wear tested under identical conditions.

It was desirable to compare wear test results with the literature when possible. Yang and Chung [5] reported results on a bauxite-reinforced aluminium casting alloy. Table VII compares the rolling wear test data of Yang and Chung with the wear test data of this study. It is difficult to compare results from other wear test data unless the test conditions are identical. In this case Yang and Chung's samples were 14 mm diameter, were tested in a fixture that held three samples, and were tested for 5000–10 000 cycles at 72 r.p.m. The samples from Table VII were 35 mm diameter, were tested one sample at a time, and were tested for 240 h

TABLE VI Comparison of metal-matrix composite modulus of elasticity values[a]

	Modulus of elasticity (GPa)		
	As-fabricated	300 °C[b]	600 °C[b]
Al/TiB_2 61 vol %	160 (14.2)	171 (56.4)	222 (40.0)
Al/SiC 55 vol % [14]	183.4 (15.0)	–	257.2 (12.4)
Al/AlN 58.6 vol % [14]	144.3 (4.2)	–	–
Al/AlN 62 vol % [14]	161.6 (0.9)	163.1[c] (1.5)	162.3 (0.6)
Al/AlN 63.3 vol % [14]	163.5 (36.5)	–	–
Al/Al_2O_3 61.4 vol % [14]	161.6 (6.9)	–	159.7 (10.8)
Al/Al_2O_3 70.2 vol % [14]	181.4 (10.8)	–	–

[a] Standard deviations are shown in parentheses.
[b] Tested at room temperature after heating.
[c] Exposed to 300 °C for 210 h, rather than 240 h for all other heated samples.

TABLE VII Rolling wear resistance expressed as relative wear.

Sample	Heat treatment	Sample volume loss (cm^3)	Wear relative to 1020 steel (%)	Wear relative to 170.1 Al (%)
Al/TiB_2 61 vol % composite	As-fabricated	0.158	0.46	0.078
Al/TiB_2 61 vol % composite	600 °C for 10 h	0.167	0.49	0.082
2024 aluminium	As-received	1.188	3.45	0.586
170.1 aluminium	As-fabricated	2.028	5.89	1.000
W1 tool steel	As-received	0.072	0.21	0.036
17-4 ph stainless steel	As-received	0.235	0.68	0.116
50 vol % Al/AlN composite	As-fabricated	0.482	1.40	0.238
1020 steel	As-received	0.344	1.00	0.170
1040 steel	Fully hardened	–	1.00[a]	–
1040 steel	Fully annealed	–	1.22	–
Al–12Si–1.4Cu–1.3Mg	As-fabricated	–	4.35 [5]	–
15 vol % bauxite-reinforced Al–12Si–1.4Cu–1.3Mg matrix	As-fabricated	–	2.69 [5]	–
20 vol % bauxite-reinforced Al–12Si–1.4Cu–1.3Mg matrix	As-fabricated	–	2.00 [5]	–

[a] In order to compare the results of this study with those of Yang and Chung [5], an assumption is made that the relative wear of fully hardened 1040 steel is approximately equivalent to that of as-received 1020 steel.

(which was equivalent to 1036 800 cycles). The number of cycles used in the wear tests of Table VII were approximately 100–200 times greater than the number of cycles used by Yang and Chung [5]. The wear-test machine used in both studies were identical.

By considering the relative wear, a reasonable comparison between the results of the two studies was possible. This was accomplished by assuming that the wear rate of the 1040 fully hardened steel sample [5] was equivalent to that of the 1020 as-received steel sample in this study. The as-received condition of the 1020 steel refers to the cold-rolled state of this commercial material. This equating of the relative wear of 1020 and 1040 steel was reasonable, because the differences in carbon content of these low-carbon steels were primarily for structural reasons and not for wear resistance. The carbon content had to be as high as those of tool steels to appreciably affect wear rates. This study also compares the Al/TiB_2 wear to the wear of the original alloy matrix. This comparison was done in order to show the increase in wear resistance which the TiB_2 addition provided over the original aluminium used.

As can be seen from Table VII, increasing amounts of bauxite increased the wear resistance. When the wear resistance of Al/TiB_2 with 61 vol % TiB_2 was compared to that of Al/bauxite, it was seen that the former experienced about 2.0–2.5 times less wear than the latter. There were many reasons for this difference, including the high volume fraction of TiB_2 particles versus the relatively low bauxite content. Another reason may be that the foundry alloy Al–12Si–1.4Cu–1.3Mg used in the bauxite composite, being of high silicon content, was more brittle than the almost pure 170.1 aluminium alloy used in the TiB_2 composite, and may be more prone to the cracking mechanisms that increased wear rates. Moreover, the two tests were run at two vastly different numbers of cycles.

Included in Table VIII are lubricated rolling wear tests from Caracostas *et al.* [6]. There were too many differences between that study and the present one to make a direct comparison. Some of the differences were the use of lubrication [6], much higher normal force of 1111 N (versus 9.8 N used in this study), a nodular cast iron rotating wheel rather than a bonded silicon carbide wheel used here, and a much shorter rolling distance of 5500 m instead of 97716 m for this study. Other differences between Caracostas *et al.*'s study [6] and the present are found in the experimental set-up. A wheel-on-cylinder apparatus was used by Caracostas *et al.*, whereas this study used a wheel and a rotating platform; a different aluminium matrix (2024 versus 170.1 in this study) was used. Even though these differences exist, we note the large difference that lubrication made in lowering the wear rate. This is true, despite a loading difference that is more than 100 times greater than that of this study.

Fig. 6 shows a scanning electron micrograph of the worn surface of the as-fabricated 61 vol % titanium diboride composite. This whole area was within the wear path and none of the surface free of wear was shown. A small piece of copper was attached to the right side of the sample to act as a marker in area location at different magnifications. This piece of copper is identified by the letter C in Fig. 6. Two distinct areas of wear appear in this photograph and were

TABLE VIII Rolling wear resistance expressed as mm^3 wear/abrasive wheel travel/9.8 N force (1 kg load)

Sample	Heat treatment	Second body rotating wheel	Lubrication	Wear rate ($mm^3 m^{-1}$)
61 vol % TiB_2/170.1 aluminium composite	As fabricated	Bonded SiC	None	1.6×10^{-3}
61 vol % TiB_2/170.1 aluminium composite	600 °C for 10 h	Bonded SiC	None	1.7×10^{-3}
2024 aluminium	As-received	Bonded SiC	None	1.22×10^{-2}
170.1 aluminium	As-fabricated	Bonded SiC	None	2.08×10^{-2}
Al–12Si–1.4Cu–1.3Mg	As-fabricated	Bonded SiC	None	1.040×10^{-1}
W1 tool steel	As-received	Bonded SiC	None	7×10^{-4}
17-4 ph stainless steel	As-received	Bonded SiC	None	2.4×10^{-3}
50 vol % Al/AlN composite	As-fabricated	Bonded SiC	None	4.9×10^{-3}
1020 low-carbon steel	As-received	Bonded SiC	None	3.5×10^{-3}
4 vol % bauxite-reinforced Al–12Si–1.4 Cu–1.3Mg matrix [5]	As-fabricated	Bonded SiC	None	6.5×10^{-2}
15 vol % bauxite-reinforced Al–12Si–1.4Cu–1.3Mg matrix [5]	As-fabricated	Bonded SiC	None	5.5×10^{-2}
20 vol % bauxite-reinforced Al–12Si–1.4Cu–1.3Mg matrix [5]	As-fabricated	Bonded SiC	None	5.2×10^{-2}
10 vol % 1.3 μm TiB_2/2024 aluminium composite [6]	T4 heat treatment	Nodular cast iron	Lubricated	2.78×10^{-5}
10 vol % 0.3 μm TiB_2/2024 aluminium composite [6]	T4 heat treatment	Nodular cast iron	Lubricated	15.4×10^{-5}
5 vol % 0.3 μm TiB_2/2024 aluminium composite [6]	T4 heat treatment	Nodular cast iron	Lubricated	17.9×10^{-5}
20 vol % 3 μm SiC/2024 aluminium composite [6]	T4 heat treatment	Nodular cast iron	Lubricated	7.63×10^{-6}
20 vol % 17 μm SiC/2024 aluminium composite [6]	T4 heat treatment	Nodular cast iron	Lubricated	3.31×10^{-5}
20 vol % 35 μm SiC/2024 aluminium composite [6]	T4 heat treatment	Nodular cast iron	Lubricated	5.41×10^{-5}

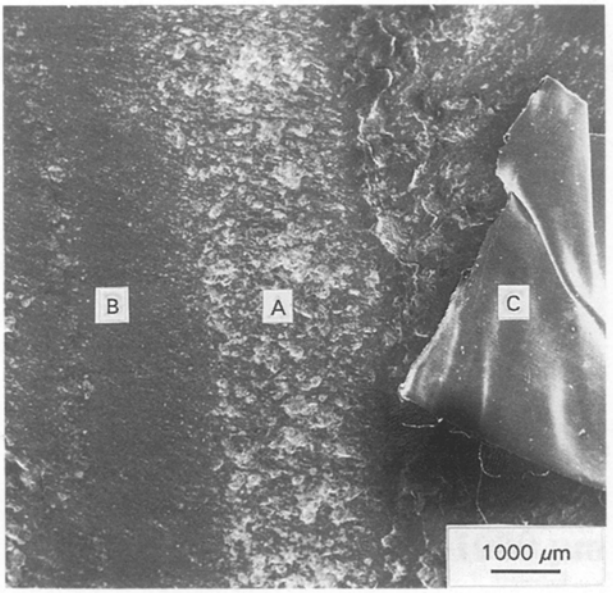

Figure 6 Scanning electron micrograph of the as-fabricated Al/TiB_2 composite with 61 vol % TiB_2. The copper foil on the right side of the photograph was used as a location point.

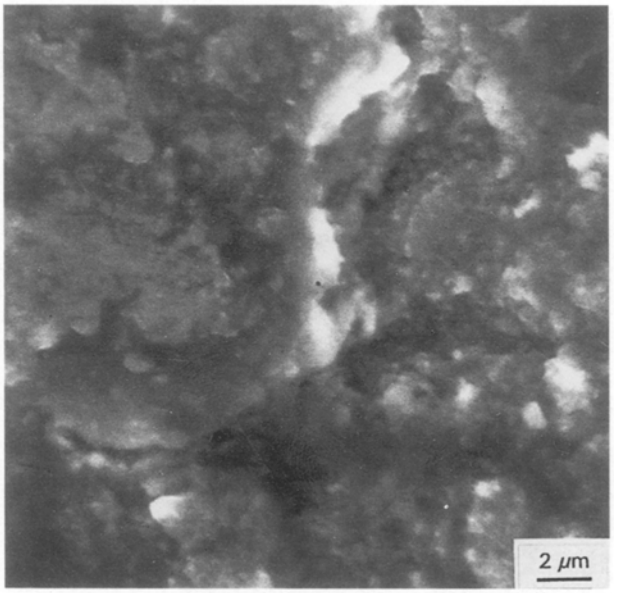

Figure 7 Scanning electron micrograph of the as-fabricated Al/TiB_2 composite with 61 vol % TiB_2. This photograph is a close-up view of area A in Fig. 6.

separated by dotted lines in Fig. 6. Each area was identified by a letter (A or B).

In the first distinct area (area A), small areas, approximately 100–200 μm in width, appear to be removed at very shallow depths. These areas are shown at a higher magnification in Fig. 7, where cracking of the particles parallel to the applied wear force was in evidence. These cracks are over 20 μm in length. Because the largest TiB_2 particles did not exceed 10 μm diameter, these cracks had to span multiple particles.

Eventually these cracks weakened the adhesion of the broken particles to the composite and the particles were swept away during subsequent passes of the abrasive wheel, leaving the shallow pits discussed earlier. It is surmised that this cracking is through the particles instead of around the particles and through the mix. This conclusion is due to the fairly straight nature of the cracks. If these cracks were external to the reinforcing particles, they would travel through the interconnecting matrix and would change directions frequently as the crack wandered around the TiB_2 particles. The actual cracked particles were difficult to observe owing to the slight distortion in the wear path.

As discussed by Roebuck and Forno [17], the cracks in TiB_2 particles will eventually be deflected to travel parallel to the applied force. This will cause a shallow quantity of the matrix to be removed. As Roebuck and Forno [17] indicate, this method of wear allows the harder reinforcement to do a better job of protecting the softer matrix from wear than do composites vulnerable to particle pull-out. The small areas removed at shallow depths in region A of Fig. 6 are probably the shallow quantities of particles and matrix removed by the aforementioned horizontal deflection of the initially observed cracks.

Region B of Fig. 6 was at the same elevation as the material between the pits. It was thus an area that had lost a smaller volume of material. This area appears to have worn by the slow process of abrading the TiB_2 particles themselves. Abraded surfaces do not have dramatic features, as was seen with matrix smearing, particle fracture or particle pull-out. Instead, abrasive wear was deduced as the wear mechanism in area B for a number of reasons. In the rolling wear test using an abrasive wheel, not removing the debris loosened during the test lends itself to abrasive wear. Area B does not exhibit other wear mechanisms, such as particle cracking, particle pull-out or matrix smearing. The surface of region B appears relatively smooth and shows less wear than area A. It is possible that this portion of the wear track is less heavily loaded than the middle of the wear track (represented by area A).

Another reason for less wear in area B may be the lower amount of third-body particles, as the third-body particles escape the edges of the abrasive wheel. In this situation, the TiB_2 particles may have been protruding slightly above the matrix surface, protecting the soft matrix from smearing. The protruding particles, in contact with a rolling abrasive wheel, can only abrade or fracture. Abrasion of the TiB_2 particles in the matrix is a slower process than the process of particle cracking discussed earlier or the fast wear caused by particle pull-out in some composites. The two wear mechanisms discussed above appear to account for the wear resistance exhibited by the TiB_2 reinforced composite tested.

The Al/TiB_2 sample was subsequently exposed to 600 °C for 240 h and the sample surface 180° to the originally worn sample was wear tested for 240 h. Fig. 3 shows a sketch of the two faces of the wear-test samples. Face 1 is the original wear tested face. Face 2 is that at 180° from the originally worn surface. Face 2 of the Al/TiB_2 composite exposed to 600 °C for 240 h was the wear tested surface that was tested after heat treatment. Figs 8 and 9 are scanning electron micrographs at two magnifications of the wear surface of the Al/TiB_2 composite which had been exposed to

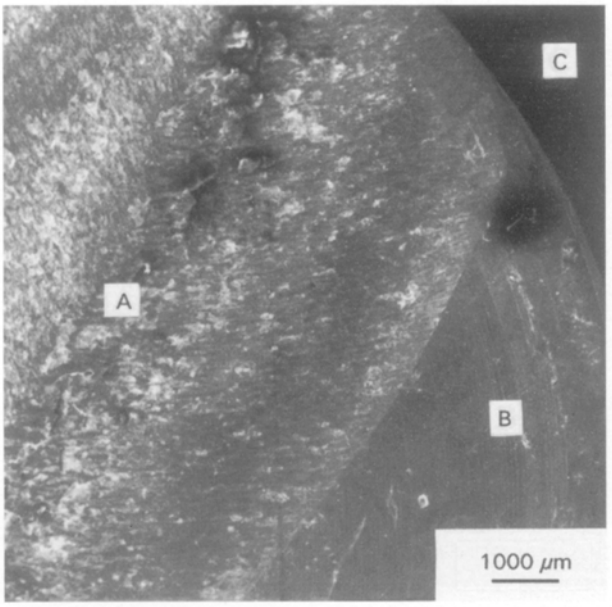

Figure 8 Scanning electron micrograph of the Al/TiB_2 (61 vol %) composite which had been exposed to 600 °C for 240 h. The area marked A is the wear path of the specimen. The area marked B is the original sample surface outside the path of the abrasive wheel. The dark area marked C is free space outside the perimeter of the sample.

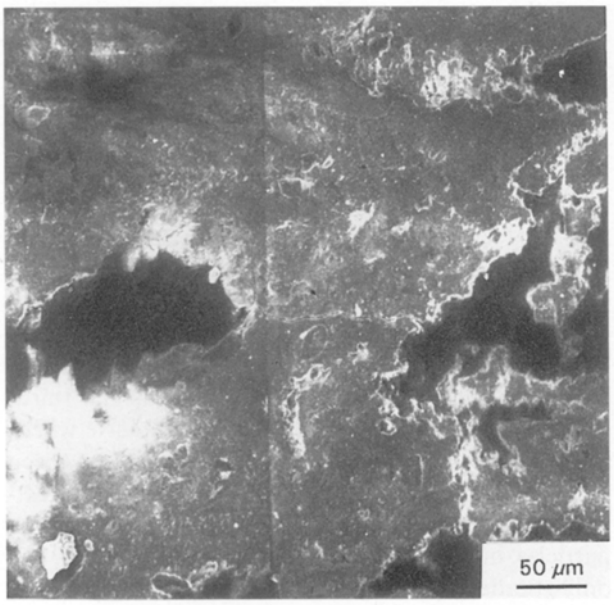

Figure 9 Scanning electron micrograph of the Al/TiB_2 (61 vol %) composite which had been exposed to 600 °C for 240 h. Fig. 9 is at a higher magnification than Fig. 8 and shows a representative part of area A of Fig. 8.

600 °C for 240 h. Note that particle cracking is evident in the centre of Fig. 9 (a horizontal crack). This crack is slightly longer than 100 μm. Because the TiB_2 particles used in making this composite did not exceed 10 μm in diameter, this crack must span multiple particles. This wear pattern is similar to that shown in Fig. 7.

For comparison, a wear-test composite sample containing AlN (50 vol %) in a 170.1 aluminium alloy matrix was wear tested. This composite was fabricated with the same equipment as the Al/TiB_2 composite

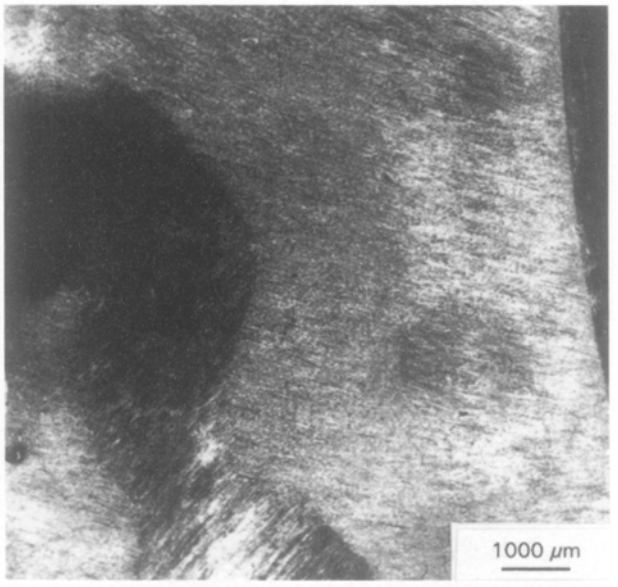

Figure 10 Scanning electron micrograph of the wear-tested surface of the Al/AlN (50 vol %) composite.

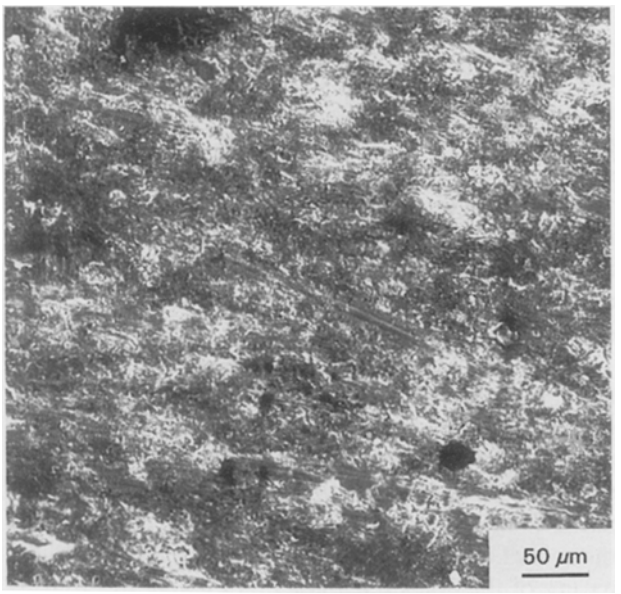

Figure 11 Scanning electron micrograph of the wear-tested surface of the Al/AlN (50 vol %) composite. Voids that appear to be caused by AlN particles pulled out from the composite were observed.

and under similar conditions. Unlike Al/TiB_2, only face 1 (Fig. 3) was wear tested. Face 2 was metallographically prepared to determine the AlN volume fraction. Fig. 10 is a low-magnification scanning electron micrograph of the worn surface of the Al/AlN sample. In this micrograph, light and dark areas are caused by uneven surfaces in the wear track. The area near the lower right corner of Fig. 10 is viewed at a higher magnification in Fig. 11, which shows voids that appear to be caused by particle pull-out. A higher magnification view shows angular walls of the hole left by particle pull-out. This supports the notion of particle pull-out. Wood *et al.* [2] indicate that particle pull-out leads to rapid wear. As the particles are removed from the composite, the softer matrix is no longer protected by the reinforcement. This appears to

be the reason why the Al/TiB_2 composite, which fails by slow particle wear, is more wear resistant than the Al/AlN composite.

The above explanation for wear resistance is an observation based on electron micrographs and does not insinuate that the filler–matrix bonding is stronger in the TiB_2 composite than in the AlN composite. Filler–matrix bonding between the matrix and TiB_2 may or may not be stronger than the bonding between the matrix and AlN. Thus differences in filler–matrix bonding may not be the reason for differences in particle pull-out tendency between TiB_2 and AlN. What is apparent here is that, before a load great enough to create particle pull-out can occur, the TiB_2 particles fracture. This dissipates the energy imparted to the sample surface by the wear test. The aforementioned particle fracture mechanism is supported by transmission electron microscope studies of the TiB_2 composite wear mechanism [16]. In comparison, the AlN particles resist particle fracture. Thus the energy imparted to the wear surface can build up enough for particle pull-out to occur.

Comparing wear-test data from other reports is difficult unless the exact test method and conditions are duplicated in both studies. A recent paper discusses the lubricated sliding wear test of 15 vol % titanium diboride-reinforced 2024 aluminium produced by the XD™ process [16]. The wear test used on the XD™ processed composite was lubricated with mineral oil. A 52100 rotating steel roller, known as a ring, was in moving contact with the stationary sample, thus causing wear. In this test, it was the stationary block that experienced the sliding wear. The composite sample was formed into a 10 mm × 10 mm × 3.6 mm block. A force of 335.8 N was applied to the steel ring. The test was run for 15 h at a sliding speed of $2\,m\,s^{-1}$. No relative wear of other materials, including composites, was compared to the Al/TiB_2 composites by Caracostas *et al.* [16]. Instead, Caracostas *et al.* concentrated on the wear mechanisms for the Al/TiB_2 composites when subjected to lubricated sliding wear against steel.

Caracostas *et al.*'s [16] sample had 1.3 μm TiB_2 particles produced in the aluminium alloy *in situ* using the XD™ process. The sample was sectioned and examined with a transmission electron microscope. Results indicate that wear initially occurred rapidly until enough of the softer matrix had been eroded to expose the reinforcing particles. When these particles extended through the surface, they supported the contacting surface of the ring. (These protruding particles are known as hard asperities.) Wear then occurred much more slowly and only continued when the asperities began to fracture.

Decohesion of the particle from the matrix appears to be extremely rare in this sample. This is an important point in that composites in which wear proceeds by particle pull-out are significantly less resistant to wear than those that rely on particle fracture. Decohesion usually occurs if brittle reactions form at the interface between matrix and the particle. Caracostas *et al.* [16] list silicon carbide-reinforced aluminium as an example of a composite where particle pull-out is the major mechanism of wear.

The Al/TiB_2 composite (this work) appears to have a similar wear mechanism to those produced by the XD™ process. Again, wear is caused by slow abrasion of the TiB_2 particles or the TiB_2 asperities fail by breakage and not by particle decohesion. This can be seen in Figs 6–9. This suggests that the interface between the titanium diboride particles and aluminium is free of brittle reaction products.

Yang and Chung [5] compared the wear resistance of bauxite-reinforced aluminium to unreinforced aluminium. Bauxite is a form of alumina often used to produce aluminium electrolytically. The matrix alloy used is defined by its nominal chemistry. All percentages in the alloy are defined as weight per cents. Its composition is 12% Si, 1.4% Cu, 1.3% Mg, and the balance is aluminium. The test equipment used was identical to the test equipment used in this work. The sample size used, 14 mm, was smaller than that used in this work. This size difference should pose little comparison problem. This is because the relative wear in each study is compared to the same aluminium matrix and a low-carbon steel.

Yang and Chung [5] used a force (9.8 N) applied normal to the wear surface which was identical to this work. The bauxite contents of the samples were 3.5, 15 and 20 vol %. It can be seen from the earlier work [5] that the bauxite-reinforced aluminium alloy wears significantly faster than low-carbon steel. An unusual result is that the lower volume fraction bauxite composites resist wear better than those at higher bauxite volume fractions.

A direct comparison between the bauxite-reinforced aluminium alloy composites of Yang and Chung [5] with the titanium diboride-reinforced 170.1 aluminium alloy matrix composite wear-test results of this work is not possible. This is because the volume fraction of bauxite reinforcement is less than half of the volume fraction of TiB_2. The alloy used for the bauxite composite is also different from the alloy used for the titanium diboride composite. What can be said is that the more highly reinforced titanium diboride composites are more wear resistant than either the lower volume fraction bauxite composites or the low-carbon steel samples.

3.4. Hardness

Hardness measurements were made on all the samples used in the wear tests. The measurements were made with a Rockwell hardness tester (B scale). The hardest materials were not necessarily the most wear-resistant materials (Table IX). This can be seen when comparing Al/TiB_2 with Al/AlN. The Al/AlN composite had the highest measured hardness – even higher than the most wear-resistant material tested, W1 tool steel. Even though the Al/AlN composite had the highest hardness, both the Al/TiB_2 composite and the W1 tool steel exhibited greater wear resistance. This result is not unheard of in the field of tribology, where the actual microscopic failure mechanism under wear loading is often more important to relative wear than

TABLE IX Hardness test (Rockwell B) results

Al/TiB_2 (61 vol %) composite	Al/AlN (50 vol %) composite	2024 aluminium	1020 low carbon steel	Wl tool steel
71.5[a] ± 3.5[b]	91.8[a] ± 0.8[b]	74[a] ± 2.0[b]	73.3[a] ± 1.6[b]	84[a] ± 1.0[b]

[a] Each Rockwell hardness value is the average of three or more measurements.
[b] These values give the variation in Rockwell hardness between multiple measurements for each material.

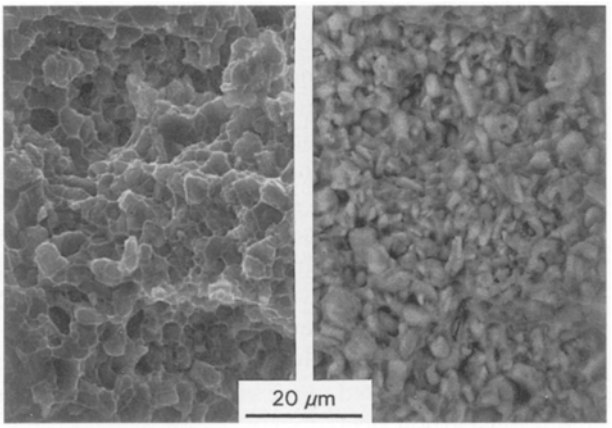

Figure 12 Tensile fracture surface of the Al/TiB_2 composite with 61 vol % TiB_2.

the actual material hardness. Hardness, in this case, is a measure of the resistance to permanent deformation due to compressive loading, and is not indicative of the wear rate.

3.5. Fracture surfaces

The fracture surfaces of the tensile test bars were observed to determine the tensile failure mode. The scanning electron micrographs in Fig. 12 are a split-screen presentation. The left part of the split screen is produced from the secondary electron image. The right part of the split screen is produced from the backscattered electron image. Similar micrographs were obtained after heating at 300 or 600 °C for 240 h. In all cases, the secondary electron image appears dimpled. These cavities are not ductile fracture dimples but are the cavities where particles resided in the matrix. For the backscattered electron image, particles that were not pulled from the tensile bar fracture surface are in evidence. In all likelihood there is a mating cavity on the mating tensile bar fracture surface where these particles used to reside. Instead of ductile failure, it appears that particle pull-out was the predominant failure mode. This is consistent with the almost total lack of elongation of the tensile specimens. No broken particles are in evidence.

4. Conclusion

The Al/TiB_2 composite with 61 vol % TiB_2 showed exceptionally good resistance to unlubricated rolling wear for 240 h continuous testing. A relative wear comparison between the TiB_2 composite and aforementioned engineering alloys and an Al/AlN composite led to the conclusion that the Al/TiB_2 composite is more wear resistant than all these materials except W1 tool steel. Wear-test results are traditionally compared to low-carbon steels. When compared to 1020 low-carbon cold-rolled steel, the Al/TiB_2 composite is twice as wear resistant. This excellent wear resistance is related to the wear mechanisms. For Al/TiB_2, the mechanisms are particle abrasion and particle fracture, which are slow processes and which cause the softer matrix to be protected by forcing most of the wear to occur on the hard TiB_2 particles protruding above the matrix.

The Al/AlN composite has a relatively low resistance to wear. Particle pull-out is the major wear mechanism. When the particles are not retained by the matrix, the matrix is exposed to rapid wear. When the TiB_2 composite is compared to 17-4 ph stainless steel, the comparative wear resistance of the composite is approximately 1.5 times greater. (The wear mechanism for stainless steel is much different. The stainless steel has a soft structure and tends to smear.)

The Al/TiB_2 composite retains much of the room-temperature mechanical and wear properties after exposure to 300 or 600 °C for 240 h. There is an approximately 10%–15% drop in ultimate tensile strength after this heat exposure. This drop occurs primarily between the as-fabricated condition and the samples exposed to 300 °C for 240 h. There is little discernible difference in tensile strength between the samples exposed to 300 and 600 °C for 240 h.

The Al/TiB_2 composite was compared to typical engineering materials, namely 170.1 aluminium, 2024-O aluminium, 2024-T6 aluminium, 1020 cold-rolled steel and 17-4 stainless steel. Even after exposure to temperatures up to 600 °C, Al/TiB_2 is equivalent in ultimate tensile strength to low-carbon steels. The Al/TiB_2 composite is slightly lower in strength than fully hardened 2024-T6 aluminium. This is a vast improvement over the unreinforced 170.1 aluminium matrix alloy and over the 2024 aluminium alloy after exposure to 300 or 600 °C for 240 h.

The Al/TiB_2 composite was also compared to other metal–matrix composites. All these composites used the same matrix alloy as the TiB_2 composite. The reinforcement loadings for each of these materials are 55 vol % SiC, 58.6 vol % AlN, 62 vol % AlN, 63.3 vol % AlN, 61.4 vol % Al_2O_3 and 70.2 vol % Al_2O_3. The Al/TiB_2 (61 vol % TiB_2) composite has a higher ultimate tensile strength than all these composites except for the composites reinforced with 62 vol % AlN and 63.3 vol % AlN. The TiB_2 composite per cent elongation is extremely low ($< 0.2\%$), as typical of ceramic-reinforced metals with a high ceramic particle loading.

Exposure to high temperatures for a long time, 300 or 600 °C for 240 h, causes a decline in room-temperature ultimate tensile strength for all composites tested. Composites used in the long-term high-temperature exposure tests are the aforementioned 61 vol % TiB_2 composite and the following other aluminium-matrix composites: 55 vol % SiC, 62 vol % AlN and 61.4 vol % Al_2O_3. By comparing the percentage decline of the ultimate tensile strength of the composite samples, the two composites made from reinforcements that do not react with the matrix (TiB_2 and AlN) exhibit $<15\%$ decline in strength. However, SiC, which forms a brittle intermetallic with aluminium, forms a composite exhibiting an 18% decline in ultimate tensile strength. Although Al_2O_3 does not react with aluminium, porosity due to particle agglomeration causes an even larger (28%) decline in the tensile strength of the Al_2O_3 composite [10]. These results indicate that reinforcements that do not react with the matrix, such as TiB_2 and AlN, are resistant to loss in room-temperature tensile strength after exposure to temperatures as high as 600 °C for 240 h, while reactive reinforcements, such as SiC, give composites that show greater loss of strength after such heat exposure.

The modulus of elasticity of the 170.1 aluminium alloy is vastly increased by the introduction of TiB_2 particles. For the Al/TiB_2 (61 vol % TiB_2) composite, the modulus of elasticity increases to as much as two to three times that of the original matrix. Exposure to long-term high temperatures, as high as 600 °C for 240 h, appears to have no detrimental effect on the modulus of elasticity for the Al/TiB_2 composite. The modulus was compared with those of typical engineering alloys. The Al/TiB_2 composite's modulus is similar to those of 1020 low-carbon cold-rolled steel and 17-4 ph stainless steel, but is two to three times higher than that of 2024 aluminium at all available tempers. When compared to the aforementioned metal-matrix composites, the TiB_2 composite in this study has similar stiffness.

In summary, aluminium–matrix composites with a high TiB_2 particle volume fraction (such as 61%) show excellent wear resistance. Owing to this wear resistance, and also to the demonstrated retention of mechanical properties after high-temperature exposure, these composites show great promise in replacing heavier steel components in weight-sensitive automotive and aerospace engines. Examples of possible applications include piston engine cylinder bores and liners, jet aircraft engine components, valve seats and valve train components.

Owing to the highly abrasive nature of the TiB_2 particles, machining of the Al/TiB_2 tensile specimens cannot be accomplished with conventional cutting tools. Only diamond saws and abrasive machining wheels can be used to prepare tensile test specimens. This extreme resistance to machining suggests that this material can be used for security purposes, such as lock shanks, automotive anti-theft devices and lightweight armour. It appears that the very property that inhibits manufacturability makes the composite attractive for niche applications such as security and light armour.

References

1. C. S. LEE, Y. H. KIM, K. S. HAN and T. LIM, *J. Mater. Sci.* **27** (1992) 793.
2. J. V. WOOD, P. DAVIES and J. L. F. KELLIE, *Mater. Sci. Technol* **9** (1993) 833.
3. *Adv. Mat. Proc.* **143** (6) (1993) 26.
4. I. M. HUTCHINGS, *Mater. Sci. Technol.* **10** (1994) 513.
5. J. YANG and D. D. L. CHUNG, *Wear* **135** (1989) 53.
6. C. A. CARACOSTAS, M. E. FINE and H. S. CHENG, in "Friction and Wear of Technology for Advanced Composite Materials" edited by P. K. Rohatgi (ASM, Metals Park, OH, 1994), pp. 79–86.
7. P. K. ROHATGI, S. RAY, Y. LIU and C. S. NARENDRANATH, *ibid.*, pp. 1–12.
8. P. K. ROHATGI and C. S. NARENDRANATH, *ibid.*, pp. 21–5.
9. W. AMES and A. T. ALPAS, *ibid.*, pp. 27–35.
10. S. LAI and D. D. L. CHUNG, *J. Mater. Sci.* **29** (1994) 6181.
11. B. K. PRASAD, S. V. PRASAD and A. A. DAS, *ibid.*, **27** (1992) 4489.
12. G. S. COLE and F. BIN, in "Friction and Wear of Technology for Advanced Composite Materials" edited by P. K. Rohatgi (ASM, Metals Park, OH, 1994) pp. 13–20.
13. J. CHIOU and D. D. L. CHUNG, *J. Mater. Sci.* **28** (1993) 1471.
14. S. LAI and D. D. L. CHUNG, *ibid.*, **29** (1994) 2998.
15. R. MITRA, W. CHIOU, M. FINE and J. WEERTMAN, *J. Mater. Res.* **8** (1993) 2380.
16. C. CARACOSTAS, W. CHIOU, M. FINE and H. CHENG, *Scripta Metall.* **27** (1992) 167.
17. B. ROEBUCK and A. FORNO, *Mod. Dev. Powder Metall.* **20** (1988) 451.
18. E. UNDERWOOD, "Quantitative Metallography" ASM Handbook, "Microstructures and Metallography", 9th Edn (ASM, Metals Park, OH, 1985) pp. 123–34.
19. T. OSBORN, Advanced Ceramics Corporation, personal communication (1993).
20. Advanced Ceramics Corporation, technical information bulletin "Titanium Diboride Powder Grade HCT" (1992).
21. H. McGANNON, (ed.), "The Making, Shaping and Treating of Steel", 9th Edn (Herbick and Held, Pittsburgh, PA, 1971).
22. K. R. VANHORN, "Aluminum", Vol. I, "Properties, Physical Metallurgy and Phase Diagrams" (ASM, Metals Park, OH, 1967).
23. Aluminum Company of America, foundry ingot technical pamphlet.

Received 8 January
and accepted 18 March 1996